JOURNAL OF MATERIALS SCIENCE 28 (1993) 773–780

Interlaminar fracture (model II) of commingled yarn-based GF/PP composites

LIN YE*, K. FRIEDRICH
Institute for Composite Materials Ltd, University of Kaiserslautern, 6750 Kaiserslautern, Germany

A 50 : 50 wt % mixture of commingled glass/polypropylene fibre system was selected to study the correlations between the morphological details, mode II interlaminar fracture toughness and corresponding failure mechanisms. Mode II interlaminar fracture tests were performed by using the end-notched flexure test procedure. Compared to conventional composite laminates, mode II interlaminar crack extension in these commingled yarn-based composites was very stable, and extensive fibre nesting occurred along the main crack plane. Crack jumping and non-broken matrix links were observed. *R*-curve behaviour for these materials was identified and the toughness for initiation was much lower than that for propagation. Compared to mode I interlaminar fracture toughness, similar trends in effects of cooling rates and isothermal crystallizations on mode II interlaminar fracture toughness were observed. However, the effects were not as significant as those found for mode I interlaminar fracture toughness.

1. Introduction

Significant effects of cooling rates, and resulting matrix crystallinity/morphology on the mechanical properties of semi-crystalline thermoplastic composites are reflected in a large number of papers that have appeared in the literature [1–10]. The investigation of the relationships between microstructure (crystallinity/morphology) and mechanical properties is an essential step in the path towards optimum selection of materials, and in finding the optimum processing window for manufacturing of composite structures.

In order to study these mechanisms more fundamentally, a 50 : 50 wt % mixture of glass and polypropylene fibres in the form of commingled yarn, an example of the new innovative intermediate material forms, was selected to characterize the relationships between matrix morphology and mode I interlaminar fracture behaviour. It was also attempted to identify the special fracture mechanisms involved in this kind of material [11]. Here the results for mode II interlaminar fracture will be presented. Special attention is further directed to examine effects of the degree of matrix crystallinity and spherulite size on mode II interlaminar fracture resistance and to identify special fracture mechanisms involved.

2. Experimental procedure

2.1. Materials

The material used in this study was a glass fibre (GF)/polypropylene (PP) fibre commingled yarn (Toyobo Co., Japan). The fibre yarns consisted of a 50 : 50 wt % mixture of the two components. Unidirectional "prepreg" sheets as well as laminates were manufactured within a steel mould using a heat press (Fig. 1). Each laminate contained 16 layers of GF/PP films, the final thickness of the laminates was about 4.6 mm. A thin steel foil (30 μm), coated with release agent, was included between the eighth and ninth layer at one end of the laminate during the moulding in order to obtain a reasonably sharp starter crack. The mould containing the GF/PP films was first heated to 200 °C; then a compressive pressure of 1.5 MPa was applied over a period of 20 min. Depending on the thermal history preceeding the physical and mechanical tests, all the laminates were classified into the following categories (Fig. 2) [11].

1. Rapidly cooled from the melt, i.e. quasi-quenched (I, 20 °C min^{-1}).
2. Crystallized directly from the melt at low cooling rates (II, 4 °C min^{-1}; III, 1.2 °C min^{-1}).
3. Isothermally crystallized at T_c = 130 °C at different crystallization times (IV, t_c = 45 min; V, t_c = 6 h), before rapidly cooling.

2.2. Calorimetry and microscopy

Crystallinity levels and thermal characteristics of the unidirectional laminates were assessed using differential scanning calorimetry (DSC). The spherulitic morphology of the PP matrix in the laminates was studied by polarized transmitted light microscopy. Scanning electron microscopy (Jeol JEM-5400 SEM) was applied to investigate the interlaminar fracture surfaces

* Alexander von Humboldt Fellow.

0022–2461

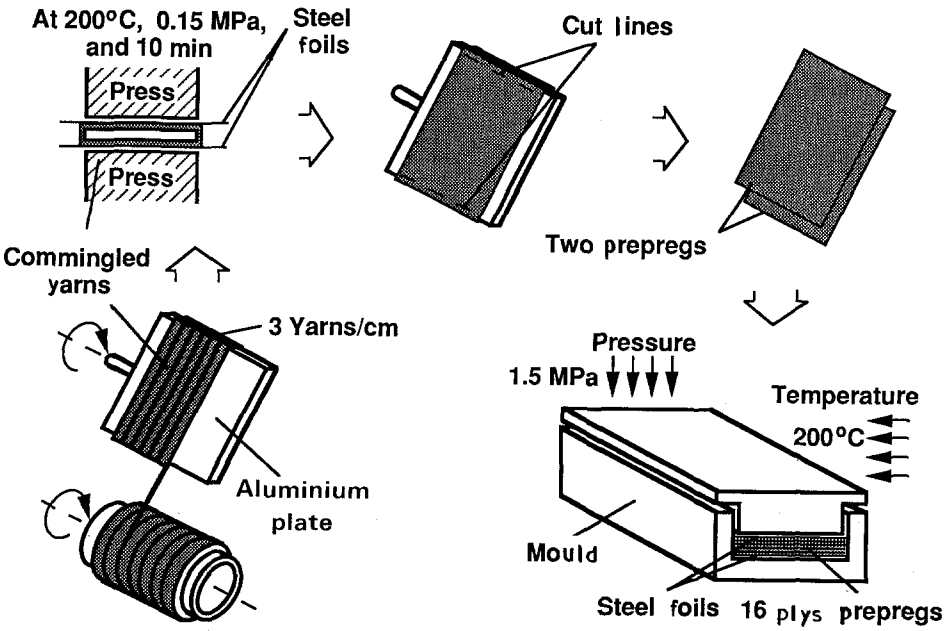

Figure 1 Manufacturing of GF/PP prepregs and unidirectional laminates from commingled yarns.

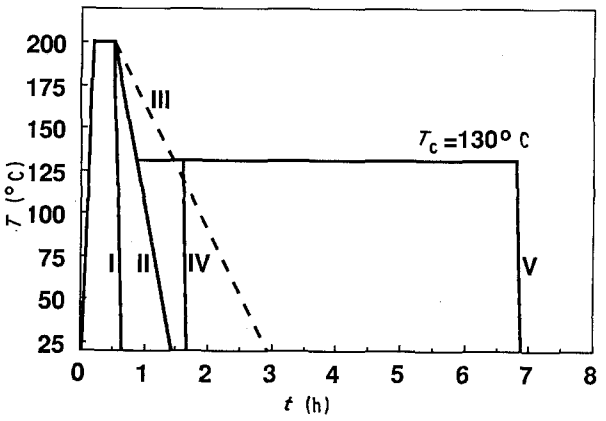

Figure 2 Thermal histories of the different GF/PP laminates.

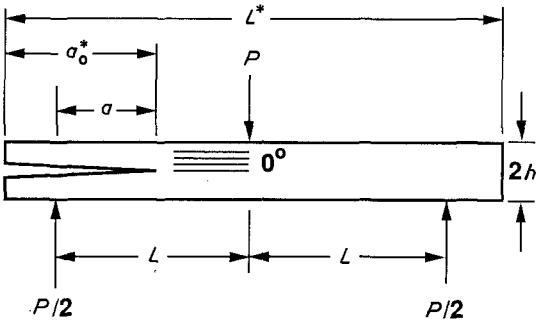

Figure 3 Schematic drawing of end-notched flexure (ENF) test arrangements.

of the laminates after mechanical testing. Details about both specimen preparations and experimental evaluations have been reported in our previous paper [11].

2.3. Mechanical testing

Mode II interlaminar fracture tests were performed at room temperature using the end-notched flexure (ENF) testing procedure (Fig. 3). Specimens were cut from undirectional laminates and then polished with abrasive papers. Their dimensions were $B = 20$ mm width and $L^* = 160$ mm length. The size of the starter crack, as induced by the steel foil, was about $a_0^* = 70$ mm; this was long enough to apply the appropriate experimental compliance calibration as a function of "insert-induced crack" length. Moving the specimen between the loading pins allowed the test to start with a ratio of 0.5 between the starter crack length and the half span ($L = 50$ mm). No effort was made to produce a "natural precrack". The specimens were loaded continuously at a crosshead speed of 1 mm min^{-1} in the Zwick 1445 static testing machine.

Load and displacement were recorded continuously, and actual crack lengths were marked every 5 mm on these records when stable crack growth occurred. A travelling microscope helped to observe the crack growth along the specimen edge. The mode II interlaminar fracture toughness, G_{IIC}, was evaluated by two methods. One of them followed the traditional "beam theory" [12]

$$G_{IIC} = \frac{9a^2P\delta}{2B(2L^3 + 3a^3)} \quad (1)$$

Another method was based on the experimental compliance calibration. A least squares linear regression was carried out for determining the compliance, C, as a function of crack length [13]

$$C = C_0 + ma^3 \quad (2)$$

Then the interlaminar fracture toughness could be evaluated from the following equation

$$G_{IIC} = \frac{3ma^2P^2}{2B} \quad (3)$$

where P is the critical load, δ the displacement, a the crack length, C_0 the compliance of the specimen without a crack, and m the slope of the line C versus a^3.

3. Results and discussion

3.1. Morphology and crystallinity

The microstructure (crystallinity/morphology) of the semi-crystalline PP matrix greatly depended on the thermal histories employed during the manufacturing of the laminates. This fact can be seen from the polarized micrographs shown in Fig. 4. The resins have normally regular spherulite texture with sharp spherulite boundaries. The smallest spherulite size was observed for the rapid cooling condition (I), and it amounted to about 10–15 μm. The lower the cooling rates, the larger became the spherulite sizes (II, III). The largest one (80–130 μm) was observed for the sample isothermally crystallized at 130 °C (V) at a longer time. No big differences in spherulite size were achieved when the isothermal crystallization time was much shorter (IV), or when the lowest direct cooling rate was chosen (III). Further discussions on the morphological details, as well as the effect of fibres, have been presented in the previous report [11]. The degree of crystallinity, X_c, of the PP matrix in the laminates subjected to the different thermal histories was evaluated from DSC analysis; results are listed in Table I. It was found that X_c was very sensitive to the thermal history, as there were obvious differences between the different morphologies. The crystallinity varied from 52% for the rapid cooling condition (I), to 70% for the longest Isothermal crystallization time (V).

TABLE I Crystallinities of PP matrix in the laminates subjected to different thermal histories (W_f is the weight fraction of fibres, ΔH_f is the heat of fusion of fully crystalline PP)

Laminates	Enthalpy of crystal melting, $\Delta\bar{H}$ (J g^{-1})	Degree of crystallinity, X_c[a]	Melting peak, T_m (°C)
I	49.5	52%	163.8
II	57.0	60%	162.0
III	62.7	66%	163.0
IV	58.9	62%	162.2
V	66.5	70%	163.1

[a] $X_c = \dfrac{\Delta\bar{H}}{(1 - W_f)\Delta H_f}$, $W_f = 0.5$, $\Delta H_f = 190$ J g^{-1}.

3.2. Crack growth behaviour

A typical load–deflection diagram for the mode II interlaminar crack growth in the $[0_8]_s$ laminates is schematically illustrated in Fig. 5. Compared to the mode II interlaminar fracture of conventional thermosetting or thermoplastic matrix composites, crack propagation was very stable in these commingled yarn-based composites, and unstable crack growth hardly occurred. It was observed in the travelling microscope that crack initiation corresponded to the point of deviation of the load–displacement curve from its linear slope at the beginning. When the a/L ratio approached 1.1, crack growth was almost arrested.

When opening the crack after the tests, it was observed that there was extensive fibre nesting. Two causes are possible for this phenomenon. First, no distinct interlaminar resin layer is available in these commingled yarn-based composites. A large number of fibres as well as fibre bundles were bridged across the intended plane of crack propagation during the

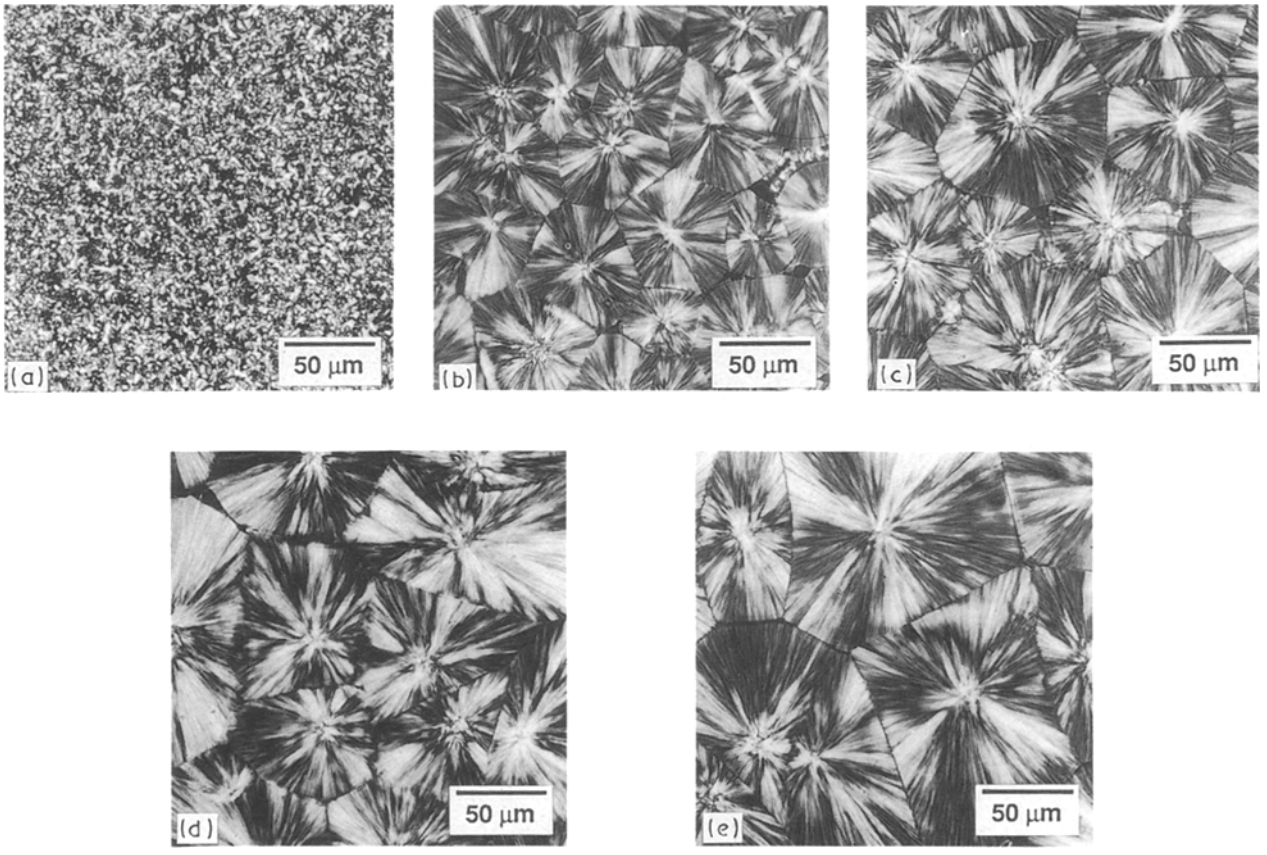

Figure 4 Polarized light micrographs of PP matrix morphologies subjected to the different thermal histories. (a) I, (b) II, (c) III, (d) IV, (e) V.

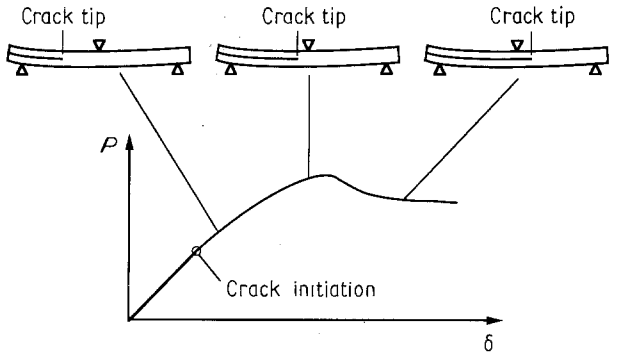

Figure 5 Typical load–deflection diagram and schematic drawing of mode II crack extension.

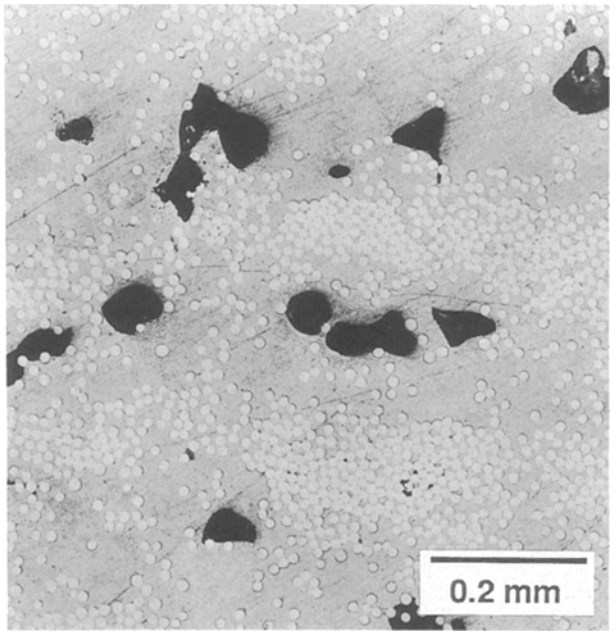

Figure 6 Micrograph of large voids in resin-rich areas when low cooloing rates or isothermal crystallizations were applied.

final laminate manufacturing. Second, PP as a highly crystalline polymer is known to undergo shrinkage upon crystallization. Thus slow cooling or isothermal crystallization conditions caused local voids at some triple points of spherulites, which in some extreme cases had grown to become large voids in resin-rich areas (Fig. 6). Loading of the materials in the vicinity of these defects (in case they exist in plies above and below the intended crack plane) may result in crack-jumping effects from the original plane into side cracks (Fig. 7). The interactions of these mechanisms contributed to the extensive fibre nesting.

Fig. 8 illustrates the cross-section of a cracked specimen; it can be clearly seen that a large number of free fibres exist between the two main crack surfaces. This again indicates the phenomenon of fibre nesting along the main crack plane. On examining the crack plane in more detail, we found that crack extension took place mainly along the fibre matrix interfaces in these fibre concentrated areas. In some resin-rich areas, on the other hand, the crack plane was not perfectly broken (i.e. matrix links still existed, as shown in Fig. 9). This means that the PP matrix can undergo much larger

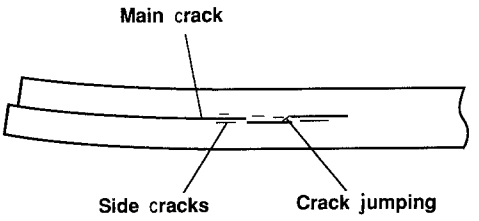

Figure 7 Schematic representation of the failure mechanisms observed.

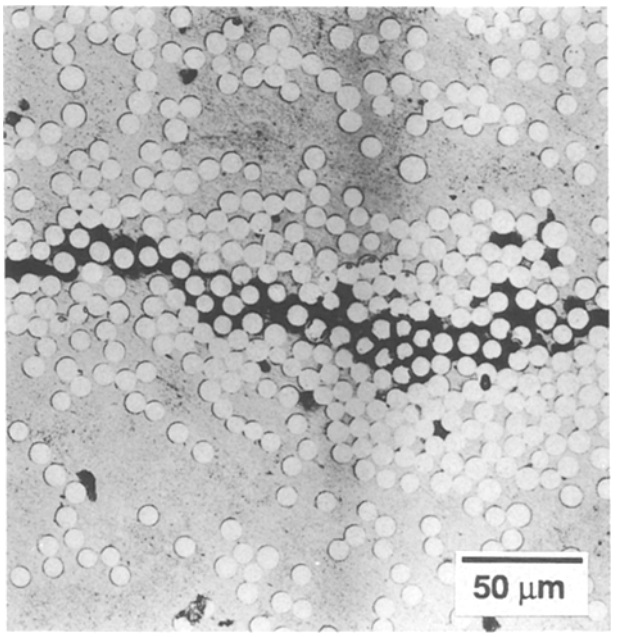

Figure 8 Cross-section of cracked specimen indicating the free fibres between two main fracture surfaces.

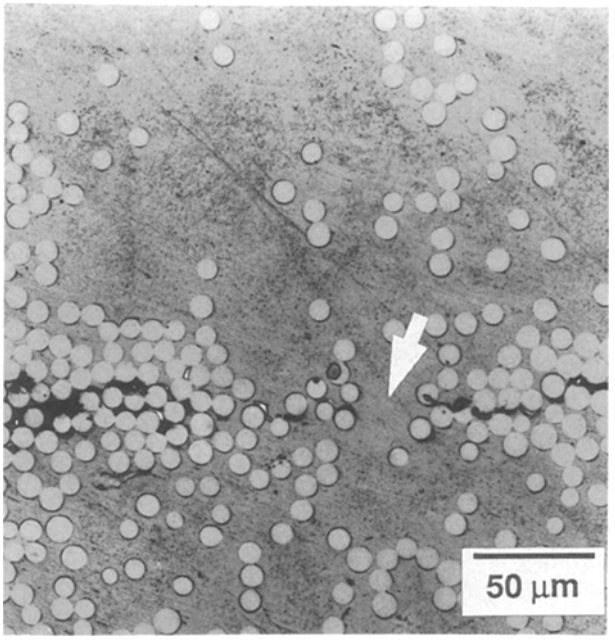

Figure 9 Unbroken matrix links (arrowed) existing in the fracture plane.

shear flow before final fracture, compared to the low interfacial bond strength between the glass fibres and the matrix.

Fibre nesting and matrix links resulted in a strong connection of the two parts of the cracked beam. After

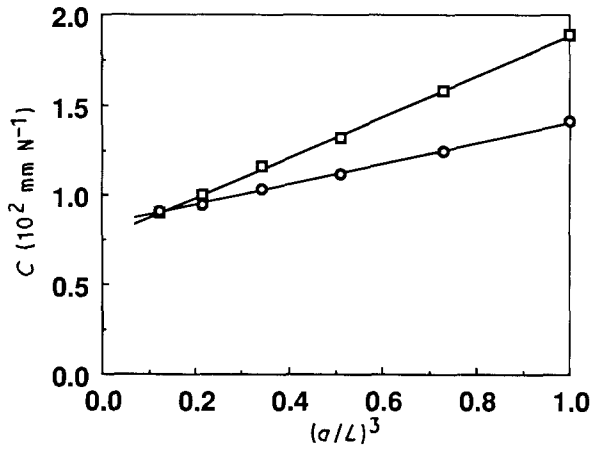

Figure 10 Compliance calibrations with (□) insert-induced crack and (○) extended crack.

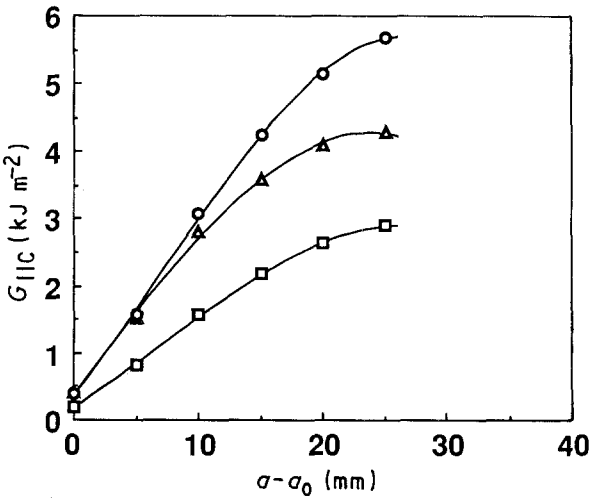

Figure 11 Comparisons between the different evaluation methods for mode II interlaminar fracture toughness. (□) Equation 3, extended crack; (○) Equation 3, insert crack; (△) Equation 1.

the tests it was, therefore, very difficult to separate the crack along the main crack plane. Fig. 10, illustrates the variations in compliance calibrations with the type of cracks (insert-induced crack and extended crack). At crack initiation, there was no obvious difference between the two compliance calibrations. But the difference became significant when the real crack extended. The compliance calibrations with insert-induced crack can be related to the response of conjugated elastic beams. It can be seen that fibre nesting and matrix links along the real crack plane resulted in a clear reduction of the beam compliance. However, in both cases, the responses of the beams can be well described by the compliance calibration procedure given in Equation 2.

3.3. Interlaminar fracture toughness

From the interlaminar fracture toughness values evaluated by the method described above, crack growth resistance curves (R-curves) can be constructed for all the laminates with different thermal histories. Fig. 11 shows the R-curves for a typical specimen of laminate type IV, as evaluated from three different procedures. First, the values were directly estimated from Equation 1; second, they were evaluated from Equation 3 and use of the experimental compliance calibrations from the insert-induced crack, which were made before the fracture tests by moving the specimens between the loading pins; and finally from Equation 3 with the experimental compliance calibrations from the extended crack. It can be seen that the differences between the values evaluated from Equations 1 and 3 with the insert-induced crack were very small only for the short crack extension. Regardless of this fact, both methods overestimate the values of mode II interlaminar fracture toughness for these commingled yarn-based composites. Hence the following results are all evaluated from Equation 3 with the compliance calibrations from the extended crack. Fig. 12 shows the variations of interlaminar fracture toughness with crack growth for laminate IV. The initiation value, $G_{IIC,init}$ was evaluated in correspondence with the crack initiation point as determined from the deviation in linearity of the load–

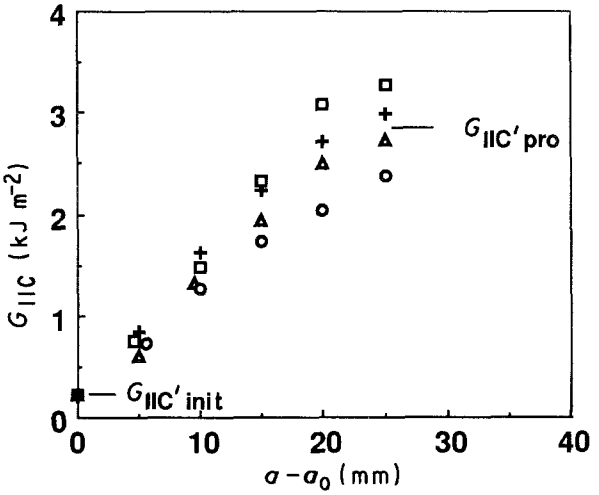

Figure 12 Mode II R-curves for laminate IV (different symbols refer to different specimens)

displacement curve. Although large scatter in the data was observed, it became clear that G_{IIC} increased quickly from the initiation value, before it approached a value designated as $G_{IIC,pro}$. This trend of the R-curves is believed to be correlated with the fibre nesting during the crack growth. From the fracture surfaces it was observed that this mechanism is not yet activated in the first loading cycle, i.e. when the crack begins to grow from the film-inserted starter crack, there is no obvious fibre nesting. With further crack advance, fibre nesting developed and fibre breaking occurred due to crack jumping and shear deformation between side cracks; thus the apparent G_{IIC} values rapidly increased with crack extension. Up to $a/L = 1$, no steady-state propagation values were identified.

From this discussion, it can be seen that the mode II interlaminar fracture toughness of a composite is not just controlled by a single material parameter, but is a result of a complex interaction of matrix, fibre, fibre geometry and their properties. The presence of R-curves of mode II interlaminar fracture toughness results from the extensive fibre nesting, which has

a significant energy contribution to the interlaminar fracture toughness.

3.4. Relation between matrix morphology and fracture toughness

Fig. 13 represents the variations of mode II interlaminar fracture toughness as a function of different matrix morphologies. Two kinds of value were involved, one was $G_{IIC,init}$, and another was $G_{IIC,pro}$, which is the value corresponding to the crack growth at a length of $a/L = 1$. The obvious trend is that smaller spherulite diameters result in greater values of interlaminar fracture toughness. For each morphology, the interlaminar fracture toughness, $G_{IIC,pro}$, in the final propagation range is at least one order of magnitude higher than that at crack initiation. The smallest spherulites corresponded to the highest interlaminar fracture toughness for both crack initiation and propagation ($G_{IIC,init} = 0.30\ kJ\ m^{-2}$ and $G_{IIC,pro} = 4.38\ kJ\ m^{-2}$), and largest spherulites resulted in the lowest ones ($G_{IIC,init} = 0.20\ kJ\ m^{-2}$ and $G_{IIC,pro} = 2.20\ kJ\ m^{-2}$).

In Fig. 14, a comparison between the mode I and mode II interlaminar fracture toughness data, $G_{IC,init}$ and $G_{IIC,init}$, as a function of matrix morphologies in these commingled yarn-based composites is demonstrated. The values of $G_{IC,init}$ were almost always higher than those of $G_{IIC,init}$. However, the general trend of the effects of matrix morphology in both modes I and II interlaminar fracture toughness is the same, although the effects in mode II are not so significant as in mode I. Fig. 15 shows the comparisions between modes I and II interlaminar fracture toughness, $G_{IC,init}$ and $G_{IIC,init}$, as a function of the degrees of crystallinity. For a change of crystallinity from 52% to 70%, reductions in $G_{IIC,init}$ by 33% were identified; the same trend was observed with regard to changes in the matrix morphology.

3.5. Microscopic observations

From the mechanical tests it can be further expected that different matrix morphologies in the composite

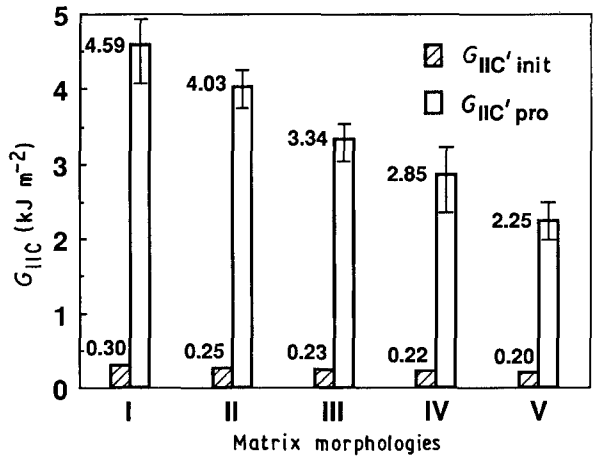

Figure 13 Interlaminar fracture toughness, $G_{IIC;init}$ and $G_{IIC;pro}$, as a function of different matrix morphologies.

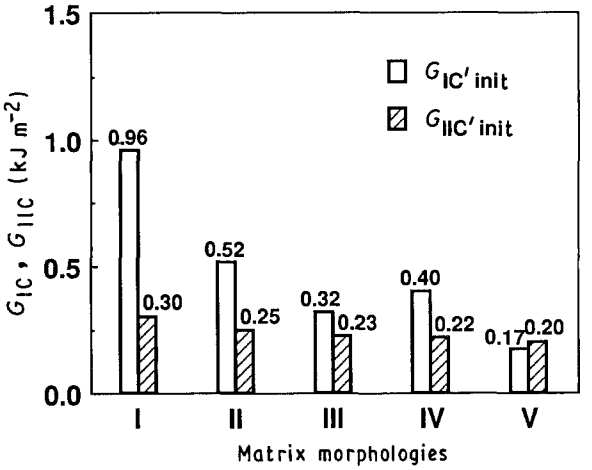

Figure 14 Comparisons of modes I and II interlaminar fracture toughness as a function of different matrix morphologies.

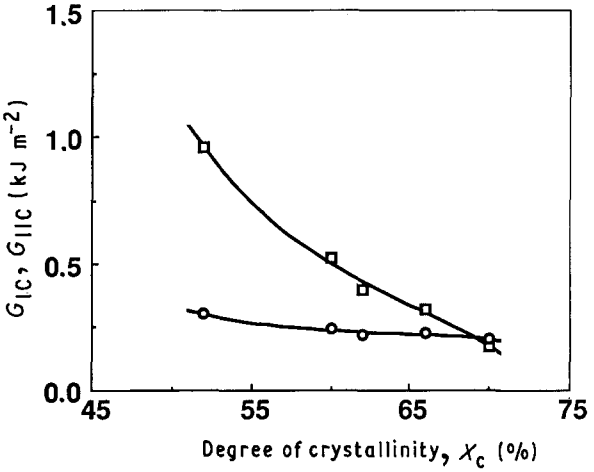

Figure 15 Comparisions of (□) mode I and (○) mode II interlaminar fracture toughness as a function of the degrees of crystallinity in PP matrix of the composite laminates.

laminates impose various crack paths during crack propagation. Figs 16–18 show scanning electron micrographs of fracture surfaces of different laminates. All of them were taken from areas near the starter crack tip, because far from this position, the fracture surfaces were closely connected by the nesting fibres and non-broken matrix links. Thus their separation did impose additional damage on the fracture surfaces. For better comparison, only the two laminates with matrix morphology I (smallest spherulite diameter) and V (largest spherulite diameter) were incorporated in this SEM illustration. Crack propagation was always from the lower left to the upper right corners of the pictures.

Fig. 16 gives an idea about the crack propagation regions preferred in the fibre concentrated areas. Although there exists a clear difference between the spherulite texture of the matrix in the two different laminates, crack propagation in these areas seems to occur mainly along the fibre/matrix interfaces. This is identical to the observations in cross-sections of the cracked specimens (Figs 8 and 9).

In contrast, Fig. 17 shows the fracture surfaces of resin-rich areas between the compacted fibre bundles. In the case of rapid cooling, the resin was subjected to

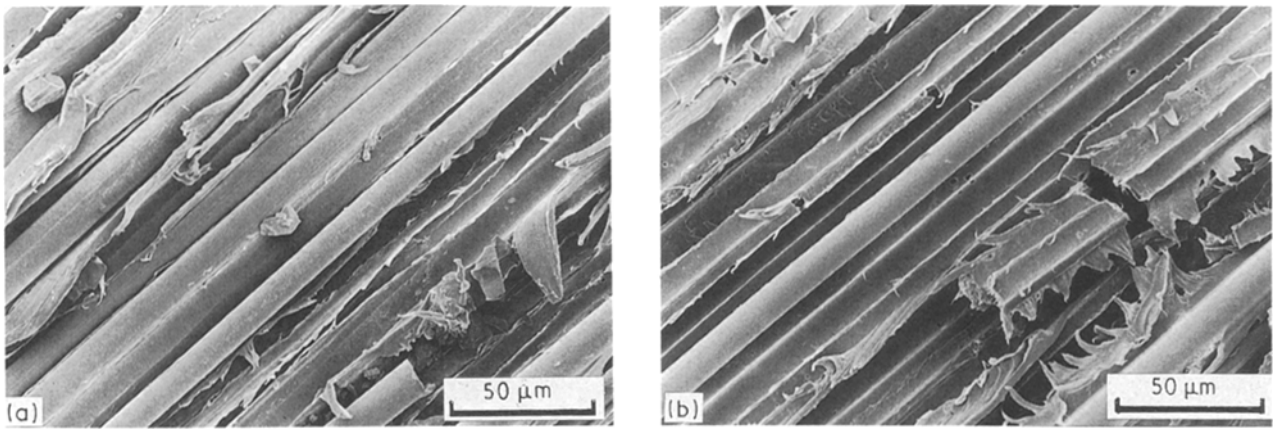

Figure 16 Scanning electron micrographs of fracture surfaces in fibre concentrated areas during crack propagation. (a) In laminate I, (b) in laminate V.

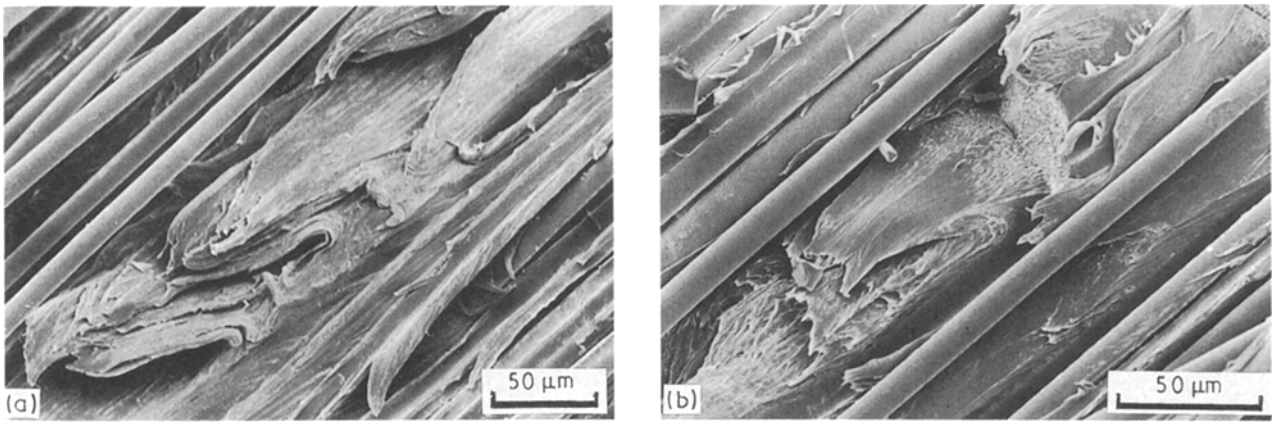

Figure 17 Scanning electron micrographs of fracture surfaces of resin-rich areas between compact fibre bundles. (a) In laminate I, (b) in laminate V.

Figure 18 Interspherulitic boundaries of large spherulites in fracture surfaces.

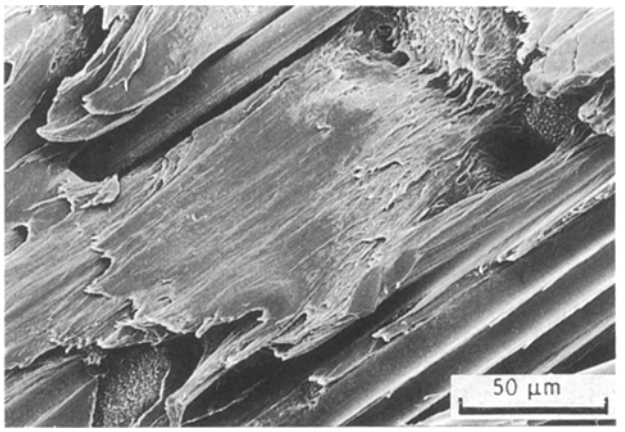

Figure 19 Scanning electron micrograph of shear failure of large of large spherulities in the laminate with morphology V.

significant shear deformations so that finally no equal dimensions between the morphological items and the fracture surface features could be identified. For specimens subjected to isothermal crystallization at elevated temperatures, on the other hand, part of the boundaries of the large spherulites appeared on the fracture surfaces (Fig. 18); this means that the paths of crack propagation were partly interspherulitic. But also here, many of the large spherulites failed under shear deformations (Fig. 19). Compared to the cases in mode I interlaminar fracture, the differences between the fracture morphologies in the rapid cooling and isothermal crystallization are smaller, hence the reductions in the mode II interlaminar fracture toughness are not as significant as those in the mode I interlaminar fracture.

4. Conclusion

The effects of processing conditions on the mode II interlaminar fracture toughness of commingled yarn-based GF/PP composites were demonstrated. Compared to the mode I interlaminar fracture toughness, the general trend of effects of matrix morphology on the mode II interlaminar fracture toughness was the same, but the effects were not so significant as those observed under mode I conditions. Rapid cooling processes resulted in greater values of the mode II interlaminar fracture toughness, whereas slow cooling rates and isothermal crystallization at elevated temperature caused lower values of G_{IIC}.

Compared to conventional composite laminates, mode II crack extension in the ENF specimens made of these commingled yarn-based GF/PP composites was very stable. A number of failure processes were observed during stable crack propagation. In particular, there were extensive fibre nesting effects along the main crack plane. Crack jumping and non-broken matrix links were observed. It has been found that the energy contributions of fibre nesting to interlaminar fracture toughness during stable crack propagation are much greater than those coming directly from matrix deformation and fracture.

Microscopic studies indicated that there existed resin-rich and fibre concentrated areas in the fracture surfaces. When the composites were subjected to low cooling rates, large voids and coarse spherulites built up in the resin-rich areas. These features resulted in partly inter-spherulitic fracture paths, and as a result of this fact the interlaminar fracture toughness for crack propagation was very much lower than that achieved for specimens prepared under rapid cooling conditions.

Acknowledgements

We thank Toyobo Co., Japan, for supplying the testing materials. Dr Lin Ye thanks the Alexander von Humboldt Foundation (AvH) for the research fellowship at the University of Kaiserslautern. This work is also a part of the research project between the University of Kaiserslautern and the Technical University of Budapest, Hungary, supported by the AvH Foundation. Professor K. Friedrich acknowledges the financial support of the Fonds Der Chemischen Industrie, Frankfurt, for his personal research activities in 1991.

References

1. W. I. LEE, M. F. TALBOTT, G. S. SPRINGER and L. A. BERGLUND, *J. Reinf. Plastics. Compos.* **6**(2) (1987) 12.
2. M. F. TALBOTT, G. S. SPRINGER and L. A. BERGLUND, *J. Compos. Mater.* **21** (1987) 1057.
3. P. CEBE, S. D. HONG, S. CHUNG and A. GUPTA, in "Toughened Composites", ASTM STP-937, edited by N. J. Johnston (ASTM, Philadelphia, 1987) pp. 342–57.
4. W. J. CANTWELL, P. DAVIES and H. H. KAUSCH, *Compos. Struct.* **14** (1990) 151.
5. P. VAUTEY, *SAMPE Q.* **21** (1990) 23.
6. R. WEISS, in "Proceedings of the Conference EACM-VI", Stuttgart (1990) pp. 1007–12.
7. P. DAVIES and D. R. MOORE, *Compos. Sci. Technol.* **38** (1990) 211.
8. B. GOFFAUX and I. VERPOEST, in "Proceedings of the Conference EACM-VI", ed. A. R. Bunsell and G. Gruninger, Stuttgart (1990) pp. 1013–18.
9. K. FRIEDRICH, *Progr. Colloid Polym. Sci.* **64** (1978) 103.
10. B. JANG, W. C. LIU, C. Z. WANG and W. K. SHIH, *J. Thermoplast. Compos. Mater.* **1** (1988) 242.
11. L. YE and K. FRIEDRICH, *Compos. Sci. Technol.* (1991) in press.
12. L. A. CARLSSON, J. W. GILLESPIE and R. B. PIPES, *J. Compos. Mater.* **30** (1986) 594.
13. L. A. CARLSSON, J. W. GILLESPIE and B. R. TRETHEWEY, *J. Reinf. Plast. Compos.* **5** (1986) 170.

Received 4 November 1991
and accepted 24 March 1992